Advanced Steel Construction – Vol. 20 No. 1 (2024) 69–80
DOI:10.18057/IJASC.2024.20.1.8

SEISMIC PERFORMANCE AND REPLACEABILITY OF STEEL FRAME STRUCTURES WITH REPLACEABLE BEAM SEGMENTS

Ling-Yun Zhao [1], Dang Guo [2], Yuan-Qiang Yang [1], Yan-Song Diao [1, *] and Xiu-Li Liu [1]

[1] *School of Civil Engineering, Qingdao University of Technology, Shandong Qingdao 266033, China*
[2] *The First Company of China Eighth Engineering Division Ltd, Shandong Jinan 250000, China*
** (Corresponding author: E-mail: diaoys@163.com)*

ABSTRACT

This study assessed the seismic performance and replaceability of steel frame structures incorporating replaceable beam segments. A reduced-beam-section beam-column joint featuring a replaceable energy dissipation beam segment was specifically designed for this purpose. The joint underwent quasi-static analysis subjected to low-cycle reciprocating loading. The study extended to a single-story, single-span plane steel frame, where reduced-beam-section beam-column joints with replaceable energy dissipation beam segments were analyzed for hysteretic and deformation behavior. Moreover, the exploration of parameters such as end-plate opening clearance and rotation deformation was undertaken to inform the simplification of the overall plane frame model. Meanwhile, multi-scale models were developed for an eight-story, four-span, reduced-beam-section steel frame (RBSSF) with a replaceable energy dissipation beam segment and a rigid steel frame (RSF). These models were employed to analyze the elastoplastic time-history characteristics and the replaceability of the beam segment. The results demonstrated that the reduced-beam-section beam-column joint with a replaceable energy dissipation beam segment exhibited a relatively full hysteresis curve, affirming high ductility, energy dissipation, and plastic deformation capacities. Notably, damage and plastic development in the steel beam primarily concentrated in the low-yield-point replaceable energy dissipation beam segment. The small end-plate opening clearance ensured cooperative deformation between the end plates facilitated by the bolts. Comparatively, the RBSSF structure displayed superior seismic performance to the RSF structure during earthquakes, with the replaceable energy dissipation beam segment satisfying replaceability requirements under moderate seismic conditions.

ARTICLE HISTORY

Received: 30 June 2023
Revised: 11 January 2024
Accepted: 29 January 2024

KEYWORDS

Multi-scale model;
Replaceability;
Replaceable energy dissipation beam segment;
Seismic performance;
Steel frame

1. Introduction

Traditional seismic structural designs typically focus on augmenting the strength, stiffness, or ductility through effective seismic measures to avoid brittle failure or collapse. However, this approach often results in plastic damage and residual deformation, presenting challenges in terms of repair [1]. Structures incorporate energy dissipation components or isolation layers to mitigate seismic responses and damage [2]. Recently, the concept of resilient structures has been introduced in seismic engineering. These structures meet the basic performance requirements and can recover and maintain functionality after an earthquake, which ensures safety, facilitates efficient post-disaster relief operations, and enables rapid reconstruction. Scholars have extensively evaluated and discussed resilient structural systems, considering various aspects such as structure, community, city, and society [3]. Resilient structures have emerged as a central focus and development direction in seismic engineering. A resilient structure [4,5] integrates rocking [6-12], self-centering [13-21], replaceable components [22-24], and additional energy dissipation devices [25-27] to diminish the structural response, damage, and residual deformation during earthquakes. The strategic placement of replaceable energy dissipation members in parallel with rocking or self-centering mechanisms contributes to diverse and resilient structural systems, maximizing their effectiveness.

Luo [28] innovatively designed a beam-column joint based on damage control principles. The joint incorporated an L-shaped plate with a stable connection to the main structure, possessing robust plastic deformation capability. This plate was the primary damage element, and its replaceability after damage was a notable feature. Shen et al. [29] conducted a quasi-static test on beam-column joints employing reduced-beam end-plate-bolted and web-channel-bolted connections. The results revealed the independent control of joint strength and stiffness, superior energy dissipation capacity for the end-plate-bolted segment, larger plastic angle for the web-channel-bolted connection, and efficient beam segment inspection and replacement after damage. Wang et al. [30] conducted experiments and numerical analysis on a reduced replaceable beam joint, demonstrating its efficacy in damage control, along with commendable hysteretic energy dissipation and replaceability. Zhang et al. [31] performed a pseudo-dynamic test on a scale sub-structure model of a web friction-type prestressed steel frame structure. Their findings showed reduced cable force loss, minimized residual deformation, and the realization of post-earthquake self-centering and structural function recovery through effective mechanisms, such as gap opening and closing and friction energy dissipation. Castiglioni et al. [32] conducted an experimental study on a beam-column joint featuring replaceable rectangular steel plate webs, confirming stable hysteretic energy dissipation characteristics and high ductility. Oh et al. [33] proposed a seismic performance-enhancing metal damper at the end of a steel beam, demonstrating effective energy dissipation and concentrated plastic deformation on a replaceable steel plate damper with a slit, leading to a favorable hysteretic performance. Shao and Chen [34] engineered a beam-column joint incorporating angle steel as the energy dissipation component, showcasing excellent hysteretic energy dissipation. Angle steel functioned as a "damage fuse" and could be readily replaced post-damage. Hu [35] introduced a high-strength steel beam-column joint with a fused connection plate, demonstrating its ability to meet load-bearing capacity demands and concentrate damage through a quasi-static test, and emphasized the pivotal role of connection plate strength in seismic performance. He et al. [36] conducted a quasi-static analysis of a beam-column joint filled with low-yield-point steel at weakened positions of the steel beam flanges and webs. The analysis indicated high ductility and energy dissipation capacity but highlighted significant buckling deformation of the steel beam. Wang et al. [37] designed a beam-column joint with a low-yield-point steel connection component, demonstrating through quasi-static analysis its effectiveness as a fuse with commendable hysteretic energy dissipation capacity. The load-bearing capacity coefficient emerged as a crucial factor influencing the joint's seismic performance. Chi and Liu [38] proposed a post-tensioned self-centering column base incorporating a buckling restrained steel plate, with a quasi-static test confirming no structural damage at a 4% rad displacement angle. The buckling restrained steel plate emerged as the primary source of energy dissipation, resulting in stable hysteretic behavior.

Current investigations into the replaceable form of steel frame structures have primarily focused on integrating various replaceable energy dissipation components at the beam end and column base. Scarce attention has been paid to researching the seismic performance and replaceability of the beam segment itself within a steel frame structure featuring a replaceable energy dissipation beam segment. Consequently, this study focused on the design of a reduced-beam-section beam-column joint incorporating a replaceable energy dissipation beam segment. The seismic performance and beam replaceability of the resulting reduced-beam-section steel frame (RBSSF) were examined, and the findings were compared with those of a conventional rigid steel frame (RSF).

2. Seismic performance of a beam-column joint with a replaceable energy dissipation beam segment

2.1. Design of the joint

The design of the reduced-beam-section beam-column joint, featuring a

replaceable energy dissipation beam segment, adhered to established standards, including the Chinese standard for the design of steel structures (GB50017-2014) [39], Chinese code for seismic design of buildings (GB50011-2010) [40], AISC 358-16 [41], and pertinent provisions and studies [29]. The specific parameters of the joint are detailed in Table 1.

Table 1
Parameters of the designed joint model

Segment	Steel beam	Column	Replaceable beam segment
Section size	H400×250×12×20	□400×400×30	H400×220×12×20
Steel grade	Q235B	Q345B	LYP160

2.2. Establishment of finite element model

In this study, we established a numerical model of the joint using the finite element software ABAQUS. The C3D8R element was employed for all members, with the normal contact direction set as "hard" and the tangent direction as the "penalty function", incorporating a friction coefficient of 0.45 [39]. The high-strength bolts followed a bilinear constitutive model, while the other steels adopted a trilinear constitutive model, as illustrated in Fig. 1. Pertinent parameters are detailed in Table 2. Von Mises yield criterion and mixed-hardening criterion [42] were selected, and the loading system adhered to the American AISC seismic code provisions [43]. The finite element model subjected to low-cycle cyclic loading translated the story drift angle into beam-end displacement. The loading amplitude curve is depicted in Fig. 2, and the node model is presented in Fig. 3.

Table 2
Material properties of the steel frame joint

Material	Stress (N/mm^2)			Strain (%)			Elastic modulus (N/mm^2)	Poisson ratio
	σ_y	σ_u	σ_t	ε_y	ε_u	ε_t	E	M
Q235	235	420	330	0.114	15	22	206000	0.3
Q345	345	554	480	0.167	25	36	206000	0.3
LYP160	160	273	230	0.077	28.6	54	206000	0.3
High strength bolt	945	1254	-	0.456	9	-	206000	0.3

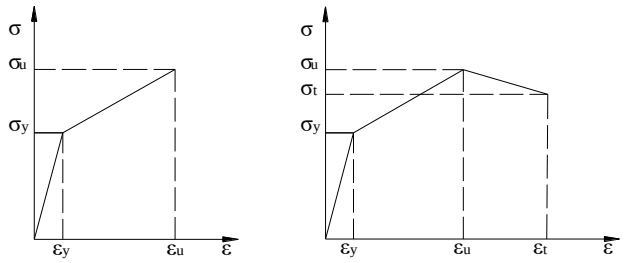

(a) (b)

Fig. 1 Constitutive model of the steel frame joint: (a) Bilinear constitutive model, (b) Trilinear constitutive model

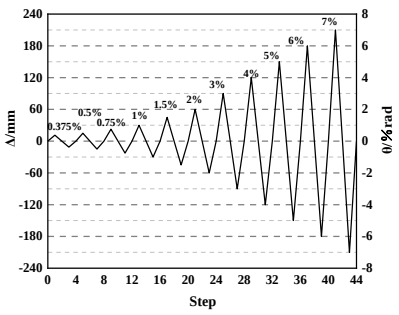

Fig. 2 Loading amplitude curve

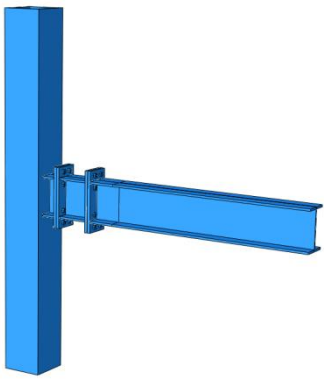

Fig. 3 Model of reduced beam section joint

2.3. Verification of the finite element modeling method

To validate the finite element model described earlier, an experimental model featuring a fabricated steel frame joint splicing a Z-shaped cantilever beam segment [44] was simulated using the finite element method. The finite element model utilized C3D8R solid elements for each segment, and other parameters and boundary conditions were derived from the reference [44]. The resulting model is depicted in Fig. 4. A comparison between the experimental and finite element simulation results is presented in Fig. 5.

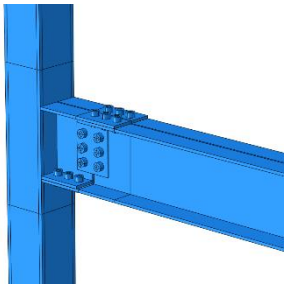

Fig. 4 Finite element model of the experimental model [44]

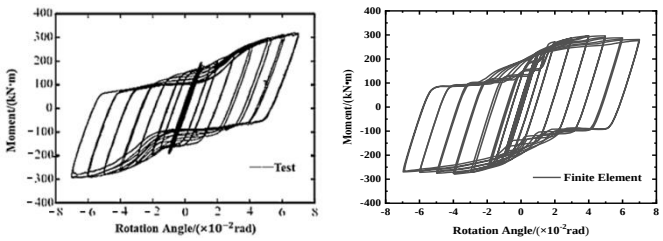

(a)

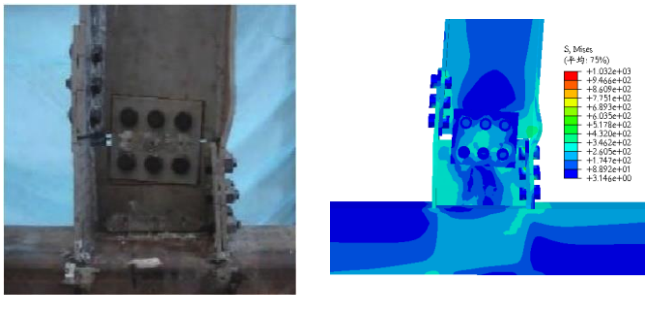

(b)

Fig. 5 Comparison between the experimental and finite element simulation results: (a) Comparison of hysteresis curves, (b) Comparison of failure modes

Fig. 5 illustrates that the hysteresis curve and failure mode of the finite element model aligned with the test results, and the simulation accurately captured the plate slip. This confirms the viability of the finite element modeling method employed in this study and establishes the reliability of the analysis results.

2.4. Results of finite element analysis

2.4.1. Hysteresis curves

The hysteresis curve depicted in Fig. 6 represents the load-displacement (P–Δ) characteristics of the designed joint under cyclic loading. The curve directly elucidates the seismic performance of the designed joint.

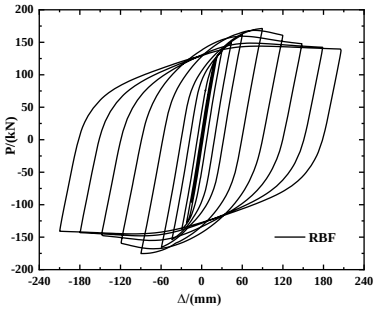

Fig. 6 Hysteresis curve of the designed joint

The joint exhibited elasticity during the initial loading stages, resulting in a small area in the hysteresis curve. As the displacement load at the beam end increased, the joint transitioned to the elastic-plastic stage, as evidenced by the decreased slope of the curve, indicating stiffness degradation. Concurrently, the load-bearing capacity and deformation increased, leading to a fuller hysteresis curve. Upon reaching the ultimate load, a further increase in the displacement load at the beam end led to a gradual decline in the joint's load-bearing capacity. Consideration of joint destruction occurred when the load-bearing capacity reached 85% of the ultimate load.

2.4.2. Backbone curve

The backbone curve represents the envelope of the load extreme points on the hysteresis curve at each loading level. It serves as a crucial reference for identifying the characteristic points of the joints. The depicted backbone curve of the designed joint is presented in Fig. 7.

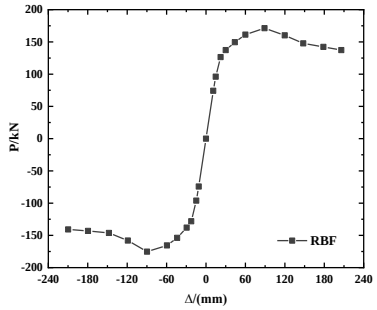

Fig. 7 Backbone curve of the designed joint

Table 3
Comparison of the load and displacement at different characteristic points

Joint type		Yield		Ultimate		Destroy	
		P_y (kN)	Δ_y (mm)	P_{max} (kN)	Δ_{max} (mm)	P_u (kN)	Δ_u (mm)
Reduced beam section	Positive	140.37	33.79	171.20	89.12	145.52	162.13
	Negative	154.13	45.33	-175.25	89.75	148.96	143.09

In Fig. 7, it is evident that the positive and negative backbone curves of the designed joint lack complete symmetry, possibly attributed to the Bauschinger effect. Initially, the backbone curve approximated a straight line during the initial loading stage. As the displacement load at the beam end increased, the slope of the backbone curve gradually decreased, deviating from a straight line. Nevertheless, the joint load-bearing capacity continued to increase, peaking at the ultimate load-bearing capacity before progressively declining until the joint failed.

In this study, the geometrography method determined the equivalent yield point of the joint. The ultimate load corresponded to the peak point on the backbone curve, with the corresponding displacement identified as the ultimate displacement. Joint failure was recognized at 85% of the ultimate load, and the associated displacement was termed failure displacement [45]. Table 3 presents a comparison of the load and displacement of the designed joint at the three characteristic points.

2.4.3. Stiffness degradation curve

Stiffness degradation denotes a gradual reduction in the specimen stiffness as the applied load increases, serving as an indicator of material damage. This phenomenon is quantified by the secant stiffness K_i [45].

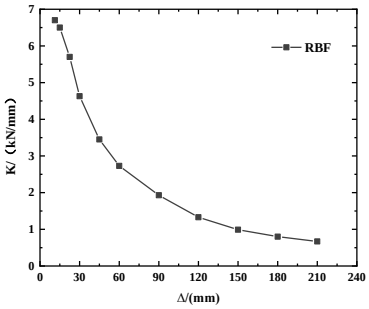

Fig. 8 Stiffness degradation curve of the designed joint

As shown in Fig. 8, the stiffness degradation curve of the reduced-beam-section beam-column joint, featuring a replaceable energy dissipation beam segment, exhibited an initial rapid decline in stiffness, followed by a comparatively slower decrease in the later stage.

2.4.4. Ductility and energy dissipation capacity

The seismic performance of joints is commonly evaluated using parameters such as ductility coefficient, total energy consumption (W_t), equivalent viscous damping coefficient (ζ_{eq}), and energy dissipation coefficient (E). These parameters are detailed in Table 4.

Table 4
Ductility coefficient and energy consumption index of the designed joint

Displacement ductility coefficient μ			W_t (kN·m)	ζ_{eq}	E
Positive	Negative	Mean			
4.79	3.16	3.98	334.45	0.48	3.01

The analysis in Table 4 revealed that the mean value of the displacement ductility coefficient (μ) for both the positive and negative directions was 3.98, indicating a high level of ductility in the designed joint. The joint exhibited an equivalent viscous damping coefficient (ζ_{eq}) of 0.48, coupled with a large hysteresis area and high total energy consumption, indicating a commendable seismic energy dissipation capacity.

2.4.5. End-plate opening analysis

This section investigated the opening and closing clearance of the joint end plate, laying the groundwork for the subsequent simplification of the overall model. Measuring points 1–9 on the joint end plate were strategically chosen for studying the opening clearance, with points 2, 4, 6, and 8 aligned with the bolt axis positions, as illustrated in Fig. 9.

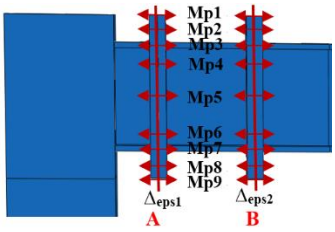

Fig. 9 Layout of measuring points (Mp)

The relationship curve, Δ_{eps}-θ_b, between the opening and closing clearances of the end plate and the beam-end rotation angle under low-cycle cyclic loading is depicted in Fig. 10. Here, the clockwise direction was considered positive for beam-end rotation, whereas counterclockwise was negative.

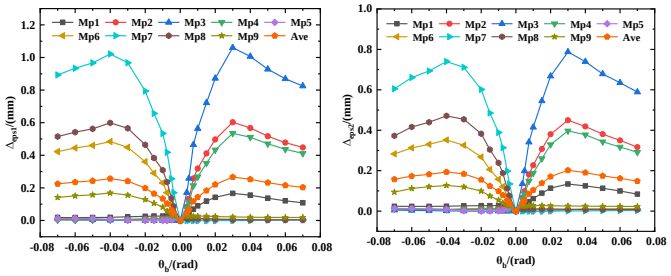

(a) (b)

Fig. 10 Relationship between end-plate opening and closing clearance and beam-end rotation angle: (a) Position A, (b) Position B

Throughout the loading process, as damage and plastic development predominantly occurred in the replaceable energy dissipation beam section, the opening clearance of the end plate remained minimal. Consequently, the bolts ensured close contact, fostered coordinated deformation between the end plates, and facilitated a stable force transfer mechanism for this connection mode.

2.5. Establishment and performance verification of the simplified joint model

2.5.1. Establishment of the simplified joint model

This section established and analyzed a simplified model of a reduced-beam-section beam-column joint featuring a replaceable energy dissipation beam segment. The coordinated deformation between the end plates, as revealed in the analysis of the joint end plate opening (Section 2.3.5) and the single-story single-span end plate (Section 3.2.2), prompted the removal of high-strength bolts in the simplified joint model based on the refined joint model. Instead, a tie constraint was implemented for the end plate contact, resulting in the simplified joint model depicted in Fig. 11.

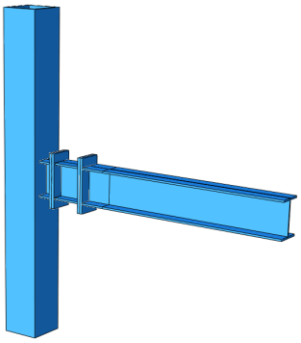

Fig. 11 Simplified joint model

2.5.2. Verification of mechanical properties of the simplified joint model

A quasi-static analysis was conducted to validate the accuracy of the simplified joint model for simulating the mechanical performance of the joint. The hysteresis and backbone curves of the simplified joint model were obtained and compared with those of the refined joint model, as illustrated in Figs. 12 and 13. Table 5 presents a comparison of the element number and calculation time between the refined and simplified joint models.

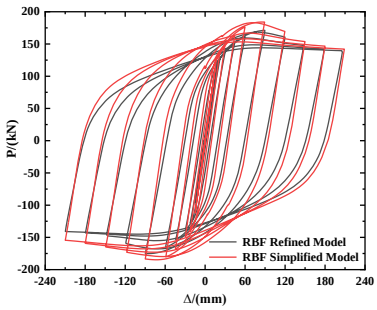

Fig. 12 Comparison of hysteresis curve of the refined and the simplified joint models

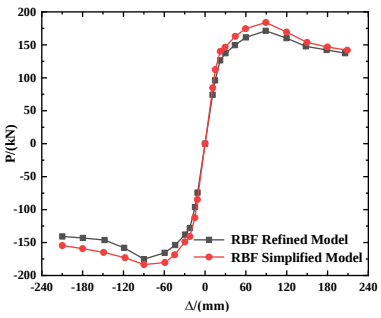

Fig. 13 Comparison of the backbone curve of the refined and the simplified joint models

Figs. 12 and 13 show a slightly higher load-bearing capacity in the simplified joint model than in the refined joint model. This discrepancy is attributed to the enhanced stiffness of the end plates resulting from the binding constraints. However, the hysteresis and backbone curves of both models were aligned, confirming the accurate simulation of the mechanical properties using the simplified joint model.

Table 5
Comparison of element number and calculation time between the refined and simplified joint models

Models	Number of elements	Calculation time (min)	Efficiency (%)
Refined model	66550	694	-
Simplified model	27430	159	336

Note: The computer for these simulations was equipped with an Intel Core i9-7980XE CPU operating at 2.6 GHz, 16 GB RAM, and an NVIDIA GeForce RTX 2080 GPU with 16 GB memory.

3. Seismic performance and end-plate deformation analysis of single-story, single-span plane frame

3.1. Establishment of finite element model

The modeling method, contact setting, and material constitutive relationship for the single-story, single-span plane frame model were consistent with those detailed in Section 2.2. To expedite convergence and reduce the computation time, connectors were utilized to streamline the representation of the bolts. Despite the advantage of eliminating the need to define the contact and mesh, connectors do not capture the response of bolts. A fixed constraint was implemented at the bottom of the column to restrict the out-of-plane displacement. Additionally, a reciprocating horizontal displacement load was applied to the column coupling point (RP-1) on the left side of the frame, as illustrated in Fig. 14. The loading system is further illustrated in Fig. 15.

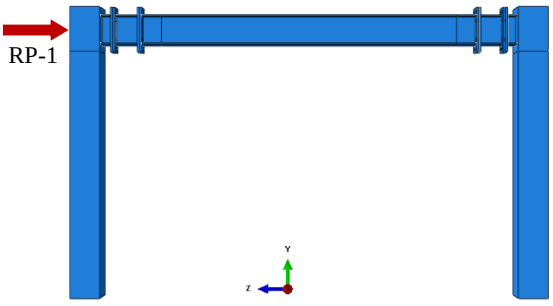

Fig. 14 Single-story single-span plane frame

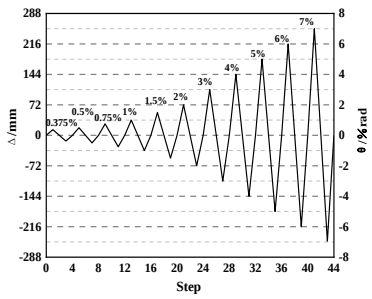

Fig. 15 Loading amplitude curve of column end

3.2. Analysis of finite element calculation results

3.2.1. Hysteresis curve

The load-displacement (P-Δ) curve of the single-story single-span plane frame is depicted in Fig. 16.

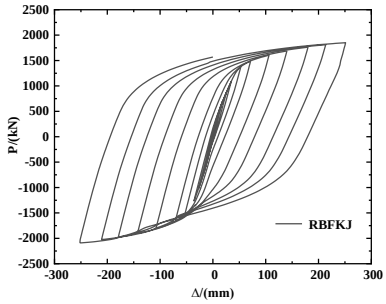

Fig. 16 Hysteresis curve of the RBF plane frame

During the initial loading stage, the plane frame structure exhibited an elastic state, resulting in a limited hysteresis curve area. As the horizontal displacement of the column end gradually increased, the structure transitioned into an elastoplastic state, accompanied by a decreasing curve slope, indicative of stiffness degradation. Simultaneously, the load-bearing capacity and deformation increased, leading to an expanded hysteresis curve. Notably, the hysteresis curve displayed a continuous shuttle-shaped loop throughout the loading process, suggesting excellent plastic deformation and energy dissipation capacity in the single-story, single-span plane steel frame with reduced-beam-section beam-column joints featuring a replaceable energy dissipation beam segment.

3.2.2. End plate opening analysis

In this section, an examination of the opening and closing clearance of the end plate was conducted, laying the groundwork for overall model simplification. Measuring points 1–9 on the end plate of the single-story, single-span plane steel frame were selected to study the opening clearance, and their layout is depicted in Fig. 17. Among these, measuring points 2, 4, 6, and 8 corresponded to the positions of the bolt axis.

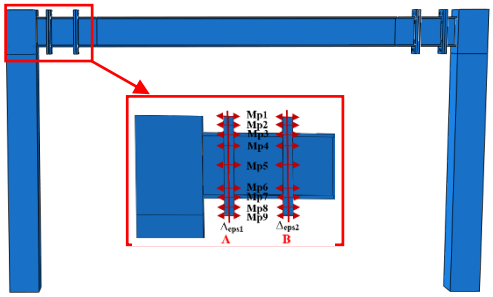

Fig. 17 Layout of opening clearance measuring points (Mp)

The Δ_{eps}-θ_c curve, depicting the relationship between the opening and closing clearances of the end plate and the beam end rotation angle under horizontal low-cycle cyclic loading, is presented in Fig. 18. Notably, the beam end rotation direction was considered positive in the clockwise direction and negative in the counterclockwise direction.

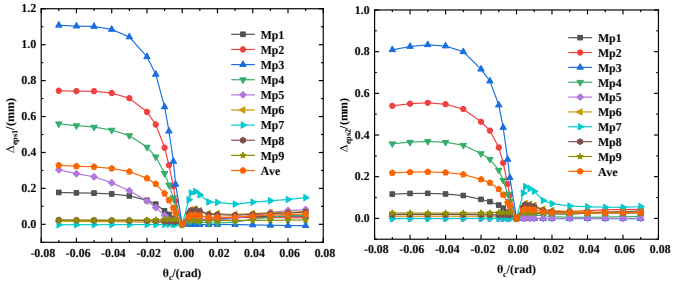

(a) (b)

Fig. 18 Relationship between the opening and closing clearance of the end plate and the beam end rotation angle: (a) Position A, (b) Position B

Fig. 18 illustrates that throughout the loading process, the opening clearance of the end plate remained minimal due to the concentration of damage and plastic development in the replaceable energy dissipation beam section of the steel beam. Consequently, the bolts ensured close contact and coordinated deformation between the end plates, facilitating a stable force transfer mechanism in this connection mode. The discrepancies in the end-plate opening and closing clearance curves between the joint and the single-story single-span plane steel frame can be attributed to the different loading positions: the joint loaded at the beam end and the frame loaded at the column end. A subsequent study of the frame structure with this joint ignored the effect of the end-plate opening.

3.2.3. Analysis of the end-plate rotation angle

In this section, the horizontal displacements of measuring points 1–9 at positions A and B of the single-story, single-span plane frame end plate are extracted and presented in Fig. 19. This study investigated the rotation angle, flatness of the end plate under different loading displacements, and replaceability of the replaceable energy dissipation beam section after an earthquake. The relationship between the end-plate height and the horizontal displacement of measuring points 1–9 (D_{ep}-Δ_{eps} curve) under varying rotation angles of the column end is depicted in Fig. 20. Furthermore, the analysis results of the rotation angle at positions A and B of the end plate are summarized in Table 6.

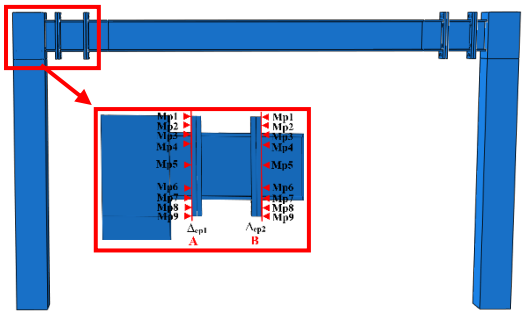

Fig. 19 Measuring points (Mp) of the end-plate displacement

Table 6
Analysis results of the rotation angle at positions A and B of the end plate

Rotation angle at column end (rad)	Rotation angle at position A (rad)	Relative rotation angle (rad)	Rotation angle at position B (rad)	Relative rotation angle (rad)
0.00375	0.0025	-0.00125	0.0013	-0.00245
0.005	0.0044	-0.0006	0.0015	-0.0035
0.0075	0.0076	0.0001	0.0008	-0.0067
0.01	0.0113	0.0003	0.0001	-0.0099
0.015	0.0181	0.0031	-0.0014	-0.0164
0.02	0.0241	0.0041	-0.0026	-0.0226
0.03	0.0353	0.0053	-0.0048	-0.0348
0.04	0.0464	0.0064	-0.0072	-0.0472
0.05	0.0593	0.0093	-0.0099	-0.0599
0.06	0.0702	0.102	-0.0125	-0.0725
0.07	0.0823	0.0123	-0.0155	-0.0855

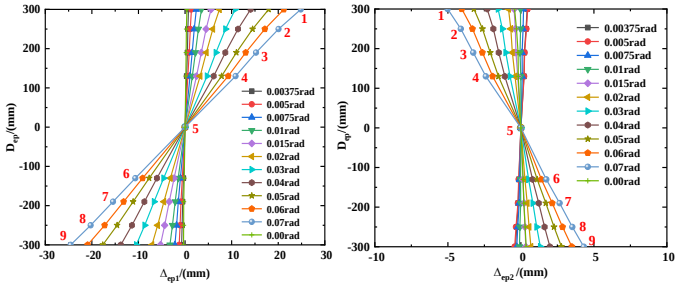

(a) (b)

Fig. 20 Displacement curve of the end plate: (a) Position A, (b) Position B

The displacements of measuring points 1–9 at positions A and B formed approximately straight lines during the loading process. This suggests the absence of significant buckling on the end plate, ensuring its flatness. Consequently, the connection between the end plates remained relatively stable, and the end plate deformation was minimal. These conditions meet the anticipated construction and replacement requirements, facilitating the post-earthquake replacement of the replaceable energy dissipation beam section.

4. Dynamic elastoplastic time-history analysis of steel frames

To assess the seismic performance of the plane steel structure featuring the designed joint, this section conducted an elastoplastic time-history analysis on an eight-story, four-span RBSSF with a replaceable energy dissipation beam segment and an RSF.

4.1. Project profile

The structure's specifications included a 4.2 m height for the bottom floor, a 3.6 m for the remaining floors, and a 6.0 m span. The seismic fortification intensity was Richter magnitude 8 (0.2 g), with a class II site classification. The designed earthquake fell under group I, with an aseismic grade of III and a designated service life of 50 years. The standard dead (live) load values were 5.0 (2.0) kN/m^2. The section sizes and steel properties of the steel beam, column, and replaceable beam segment are detailed in Table 7.

Table 7
Parameters of the steel frame

Segment	1st–3rd floor	4th–6th floor	7th and 8th floors
Frame beam	H400×250×12×20	H400×250×12×20	H400×250×12×20
Frame column	□400×400×30	□400×400×25	□400×400×20
Replaceable beam segment	H400×220×12×20	H400×220×12×20	H400×220×12×20

4.2. Establishment and validation of the multi-scale model

In this study, multi-scale modeling technology was employed to construct a nonlinear finite element model to enhance the accuracy and efficiency of the seismic performance analysis of steel frames. Multi-scale modeling integrates fine and macro models through the collaboration of different-scale elements. Previous research [46-48] has validated the feasibility of this modeling approach and the associated interface connection method.

The ABAQUS software was utilized to establish the multi-scale plane steel frame model. As shown in Fig. 21, the behavior of the replaceable beam segment and end plate was simulated using solid elements. In contrast, the shell elements modeled the behavior of the node domain and the short beam segment. Additionally, the behavior of the other frame columns and beams was represented using beam elements. The coupling command [42] ensured the connection and collaboration between the shell and beam elements.

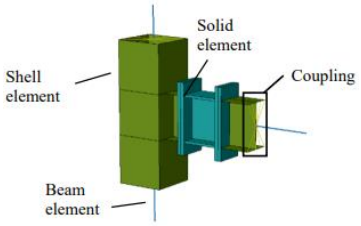

Fig. 21 Multi-scale plane steel frame models of the RBSSF and RSF established in this study for elastoplastic time-history analysis

Fig. 22 depicts the multi-scale plane steel frame models of the RBSSF and RSF established in this study for elastoplastic time-history analysis.

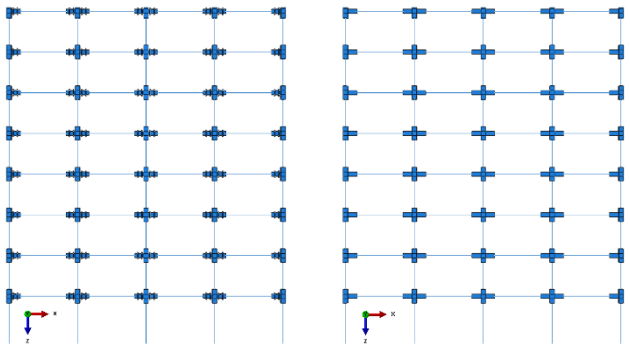

Fig. 22 Schematic diagram of multi-scale plane steel frame structures: (a) RBSSF, (b) RSF

4.3. Modal analysis

Modal analysis of the RBSSF and RSF structures was conducted using ABAQUS software. The first three-order vibration modes of the structures are illustrated in Fig. 23, and the corresponding natural vibration periods and circular frequencies for these modes are provided in Table 8.

Table 8
Natural vibration period and circular frequency of the frame structures

Frame	T_1	ω_1	T_2	ω_2	T_3	ω_3
RBSSF	1.98	3.16	0.64	9.88	0.35	18.11
RSF	1.95	3.21	0.63	10.03	0.34	18.34

Note: T_i and ω_i represent the ith natural vibration period and circular frequency of the structure, respectively.

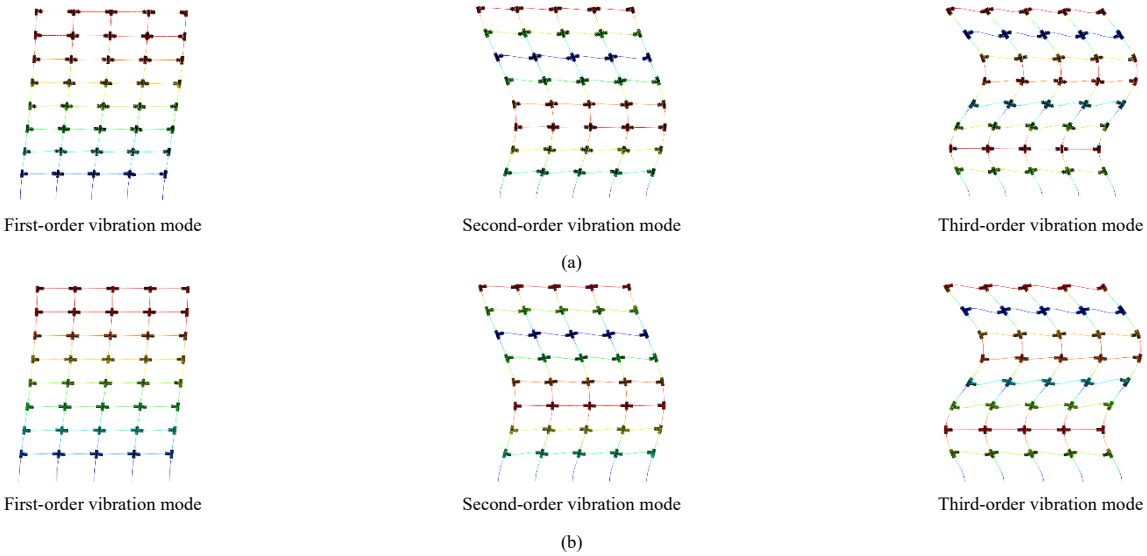

Fig. 23 First three order vibration modes of plane steel frame: (a) RBSSF, (b) RSF

In the elastoplastic time-history analysis of the structure, the impact of damping could not be disregarded. Rayleigh damping was chosen as the structural damping model in this study. The mass damping coefficient (α) and stiffness damping coefficient (β) were determined based on the natural frequency and period of the structure, as outlined in Table 9.

Table 9
Structural damping coefficients α and β

Frame	Mass damping coefficient α	Stiffness damping coefficient β
RBSSF	0.2395	0.00766
RSF	0.2434	0.00755

4.4. Selection of seismic wave

In this study, seismic wave records were meticulously chosen based on parameters such as seismic fortification intensity, seismic intensity grade, and site soil type, following the guidelines from ATC-63 [49] and the Chinese code for seismic design of buildings (GB50010-2010) [40]. Ultimately, the El Centro wave (natural wave), Westmoreland wave (natural wave), and RH4TG035 (artificial wave) were selected for elastoplastic time-history analysis. To ensure consistency in the peak acceleration with the target peak acceleration, the seismic acceleration time-history curves of the three groups of seismic waves were amplitude-modulated to 0.4 g, as illustrated in Fig. 24.

4.5. Determination of performance objectives

This study chose the maximum and residual inter-story displacement angles as the structural demand indices when subjected to earthquake motion, considering the deformation and failure criteria. The prescribed limits for the inter-story and residual inter-story displacement angles under various seismic levels were determined based on prior research [50-53] (Table 10). The scope of the residual inter-story displacement angle primarily governs the replaceability of the energy dissipation beam.

4.6. Time-history analysis results of the steel frame structure under earthquake action

4.6.1. Displacement response analysis of the top floor

The time-history curves depicting the displacement of the RBSSF and RSF structures during frequent, moderate, and rare earthquakes are presented in Figs. 25–27.

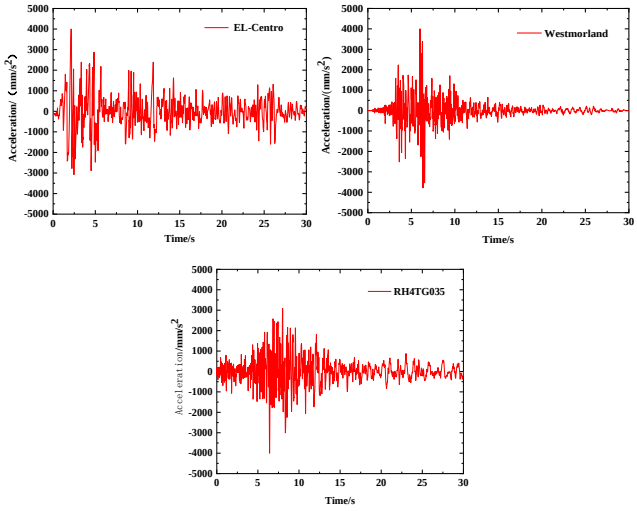

Fig. 24 Seismic acceleration time-history curves after amplitude modulation to 0.4 g

Table 10
Performance level of the steel frame structure with replaceable energy dissipation beam

Seismic level	Performance level	Structural function description	Inter-story displacement angle	Residual inter-story displacement angle
Frequent earthquake	Basically intact	The replaceable beam section may experience slight plastic deformation, while the main portion remains elastic, preserving the overall structural integrity.	< 0.4%	< 0.15%
	Slight damage		< 0.8%	
Moderate earthquake	Medium damage	The replaceable beam section incurs additional damage, with slight damage to the main portion, enabling normal functioning after replacing the damaged beam section.	< 1.2%	< 0.5%
Rare earthquake	Severe damage	The replaceable beam section sustains severe damage, leading to varying degrees of damage in the beam and column-bearing members. Partial removal of damaged members allows for the appropriate use of the structure.	< 1.8%	< 1.0%

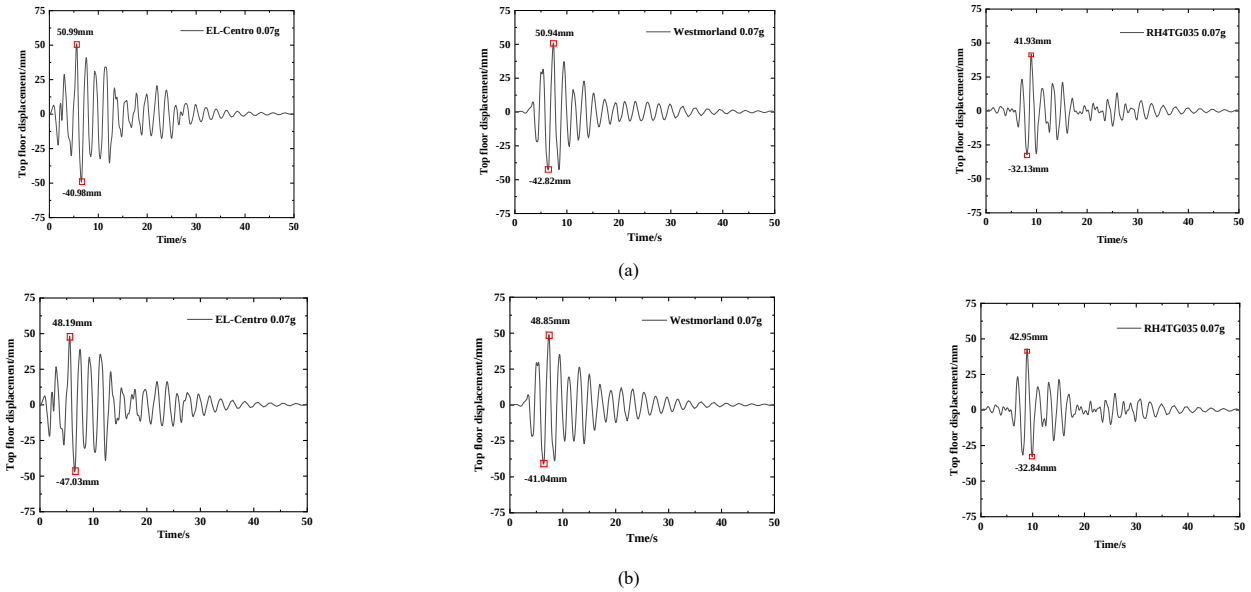

Fig. 25 Time-history curves of the top floor displacement of the steel frame under frequent earthquakes: (a) RBSSF, (b) RSF

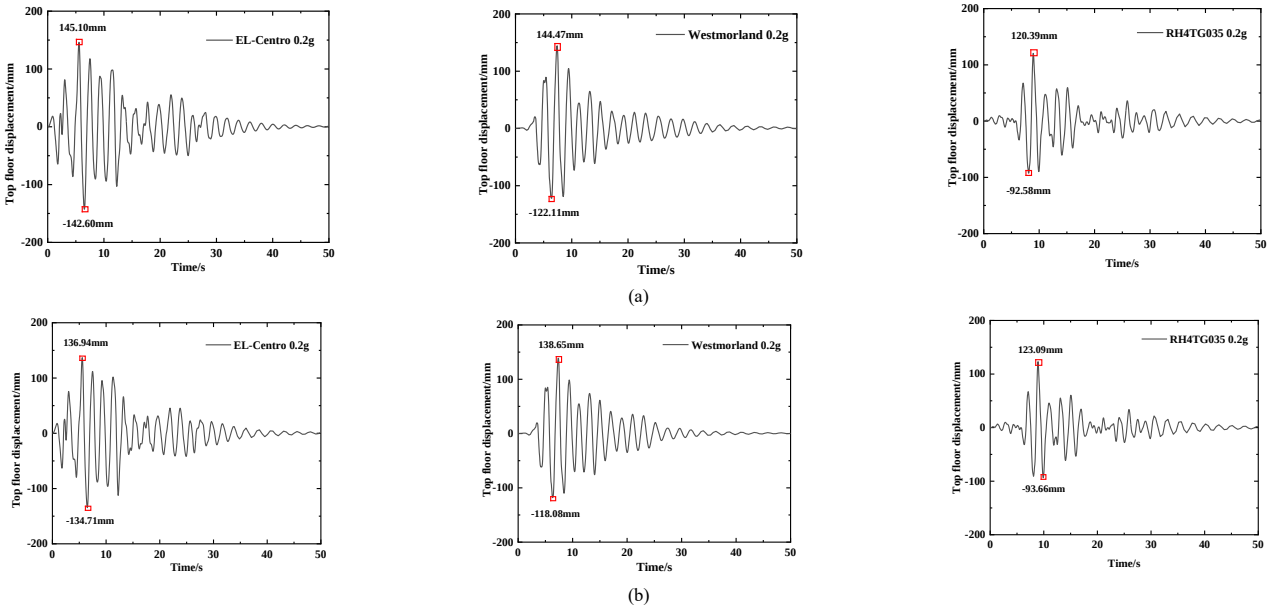

Fig. 26 Time-history curves of the top floor displacement of the steel frame under a moderate earthquake: (a) RBSSF, (b) RSF

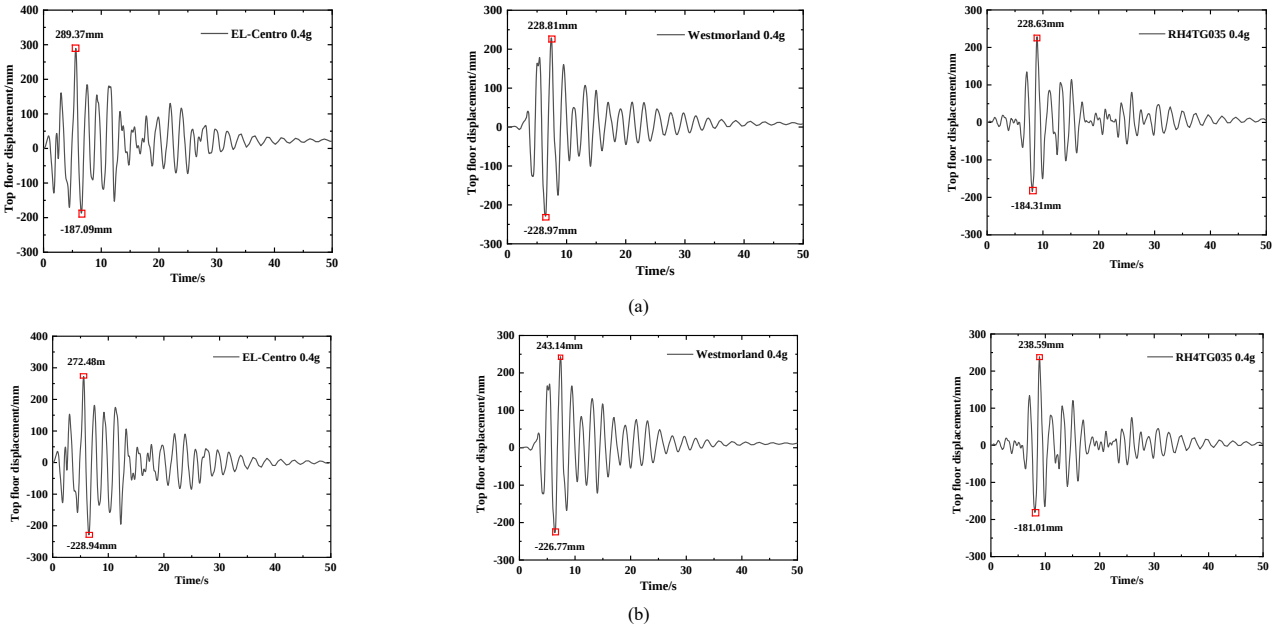

Fig. 27 Time-history curves of the top floor displacement of the steel frame under a rare earthquake: (a) RBSSF, (b) RSF

Figs. 25–27 revealed that the occurrence of the maximum displacement in the RBSSF structure lagged behind that of the RSF structure. However, the time-history curves for the top floor displacement exhibited similar trends for both the structures. Under frequent and moderate earthquakes, the maximum displacement of the RBSSF structure's top floor was slightly larger than that of the RSF structure. This discrepancy may be attributed to the RBSSF structure's reduced beam sections, resulting in an overall smaller stiffness than that of the RSF structure. Conversely, during a rare earthquake, the maximum displacement of the RSF structure's top floor slightly exceeded that of the RBSSF structure. This can be attributed to the full plastic energy dissipation of the replaceable energy dissipation beam section, with damage concentrated mainly in this section. In contrast, the primary structure of the steel frame experienced relatively minor damage.

4.6.2. Shear force response analysis of the base

The time-history curves illustrating the base shear force responses of the RBSSF and RSF structures under frequent, moderate, and rare earthquakes are depicted in Figs. 28–30.

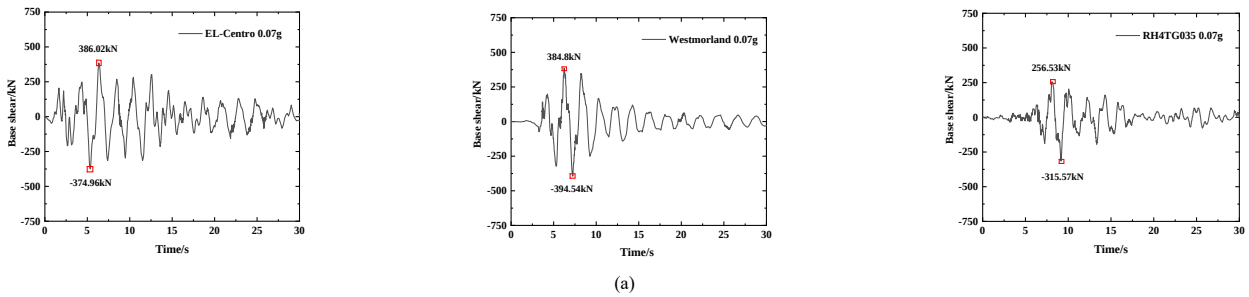

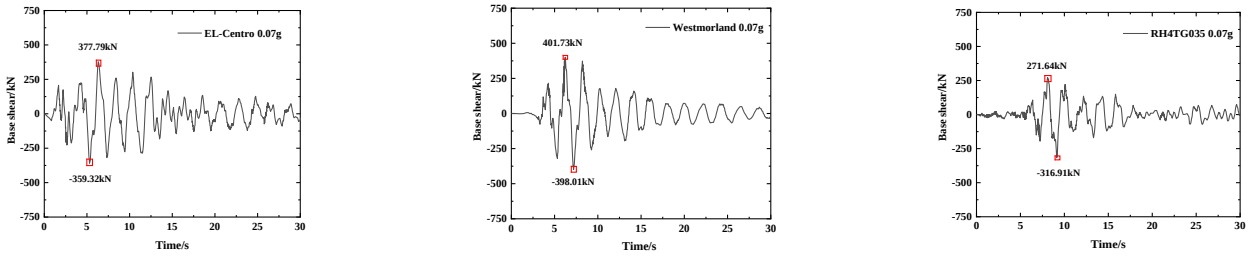

(b)

Fig. 28 Time-history curves of the base shear force of the steel frame under frequent earthquakes: (a) RBSSF, (b) RSF

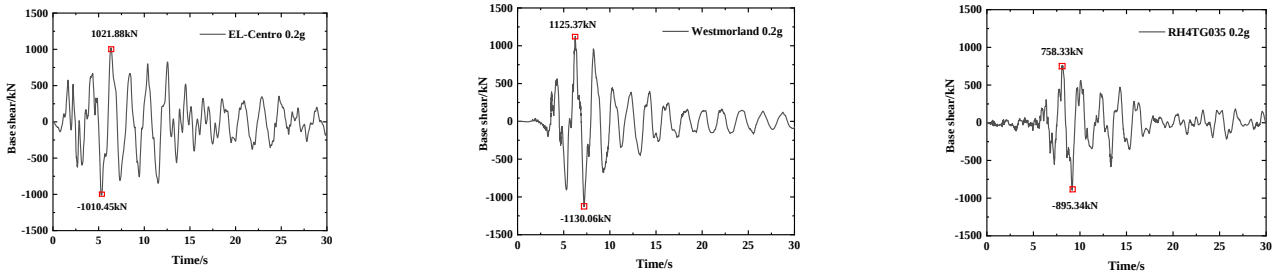

(a)

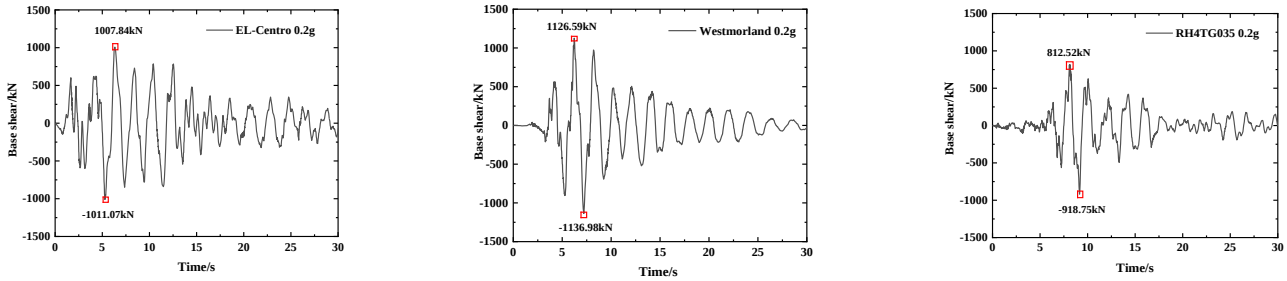

(b)

Fig. 29 Time-history curves of the base shear force of the steel frame under a moderate earthquake: (a) RBSSF, (b) RSF

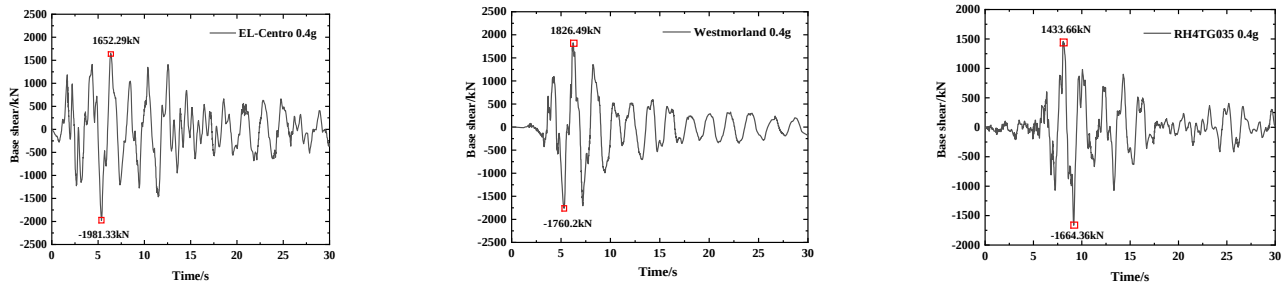

(a)

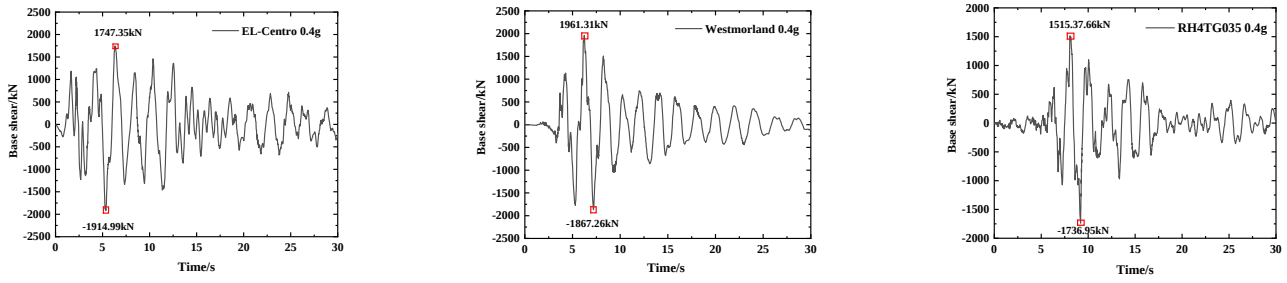

(b)

Fig. 30 Time-history curves of the base shear force of the steel frame under a rare earthquake: (a) RBSSF, (b) RSF

Figs. 28–30 show that the maximum base shear force in the RBSSF structure occurred later than that in the RSF structure under frequent, moderate, and rare earthquakes. The patterns observed in the time-history curves for the base shear forces of both structures were similar. Notably, the maximum base shear force of the RBSSF structure was marginally smaller than that of the RSF structure, contributing to a certain degree of damage reduction in the frame columns.

4.6.3. Analysis of inter-story displacement angle

The inter-story displacement angle (θ_{MIDR}) curves depicting the behavior of the RBSSF and RSF structures under frequent, moderate, and rare earthquakes are presented in Figs. 31–33.

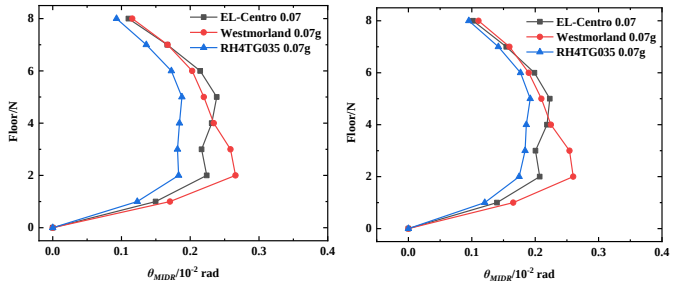

Fig. 31 Inter-story displacement angle curves of the steel frame under frequent earthquakes: (a) RBSSF, (b) RSF

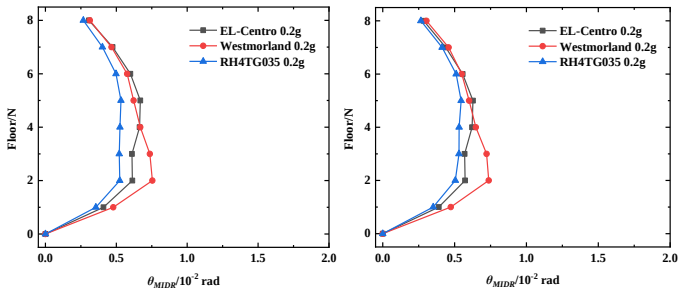

Fig. 32 Inter-story displacement angle curves of the steel frame under a moderate earthquake: (a) RBSSF, (b) RSF

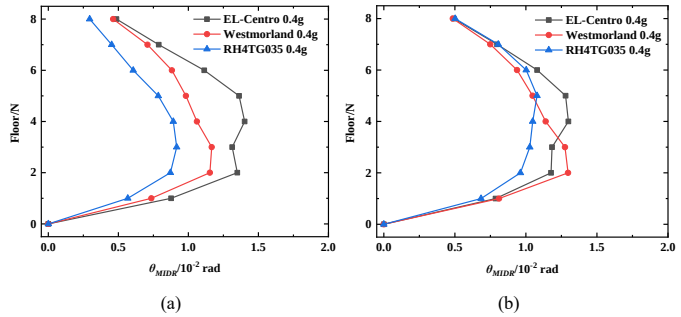

Fig. 33 Inter-story displacement angle curves of the steel frame under a rare earthquake: (a) RBSSF, (b) RSF

Figs. 31–33 revealed consistent weak floor positions and a consistent pattern in the inter-story displacement angle curves for both RBSSF and RSF structures subjected to the same seismic waves. The maximum inter-story displacement angles of both structures remained within the prescribed limits under various seismic conditions, satisfying the structural requirements. During frequent and moderate earthquakes, the RBSSF structure exhibited a slightly larger maximum inter-story displacement angle than the RSF structure. This divergence may be attributed to the full plastic energy dissipation in the replaceable energy dissipation beam section, where damage is primarily concentrated, leading to relatively minor damage and residual deformation in the main structure of the steel frame. Conversely, under rare earthquakes, the inter-story displacement angle of the RBSSF structure was relatively smaller than that of the RSF structure.

5. Feasibility analysis of energy dissipation beam replacement

Residual displacement is crucial for evaluating the seismic and toughness performance of structures and for gauging the structural recoverability and replaceability [54]. However, residual inter-story displacement provides a holistic view of the structure's overall residual deformation, lacking specificity about local residual deformation. This section analyzed the feasibility of beam segment replacement by considering the residual inter-story displacement angle and residual rotation angle of the end plate of the replaceable beam segment.

5.1. Residual inter-story displacement angle

This section extracted and analyzed the residual inter-story displacement angle (θ_{RIDR}) of the RBSSF structure. The corresponding curves under various seismic conditions are presented in Fig. 34, and detailed analysis results are provided in Table 11.

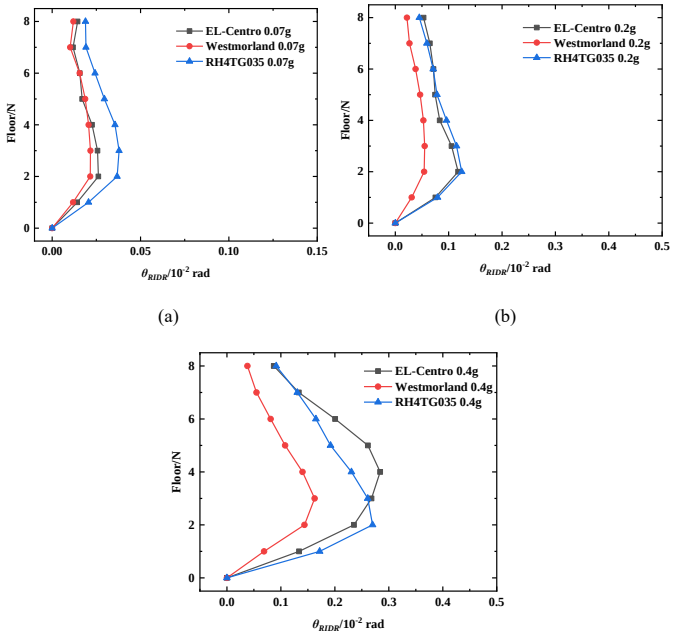

Fig. 34 Residual inter-story displacement angle curves of the RBSSF structure under earthquake action: (a) Frequent earthquake, (b) Moderate earthquake, (c) Rare earthquake

Table 11
Residual inter-story displacement angle of the RBSSF structure under earthquake action

Seismic level	Seismic wave	Floor (N)	Residual inter-story displacement angle (% rad)
Frequent earthquake	EL-Centro	2	0.026
	Westmorland	2	0.022
	RH4TG035	3	0.037
	Average	-	0.028
Moderate earthquake	EL-Centro	2	0.117
	Westmorland	2	0.054
	RH4TG035	2	0.124
	Average	-	0.098
Rare earthquake	EL-Centro	4	0.284
	Westmorland	3	0.163
	RH4TG035	2	0.270
	Average	-	0.239

From Fig. 34 and Table 11, it can be concluded that the residual inter-story displacement angle of the RBSSF structure under frequent, moderate, and rare earthquakes remained within the prescribed limits. Hence, it meets the requirements for the residual inter-story displacement angle of the structure.

5.2. Residual rotation angle of the end plate

In this section, we examined the residual rotation angle of the end plate of the replaceable beam section at the side span of the floor, where the residual inter-story displacement angle was the largest (Fig. 35). Due to the binding constraint between the end plates, the end plate exhibited relatively high stiffness, ensuring its flatness. Consequently, the analysis focused on the horizontal displacement of measuring points 1–3 at positions A and B of the end plate. The residual displacement curves (D_{ep}-Δ_{ep}) for measuring points 1–3 along the height direction of the end plates at positions A and B under different seismic conditions are illustrated in Fig. 36, with the corresponding analysis results of the residual rotation angle of the end plate presented in Table 12.

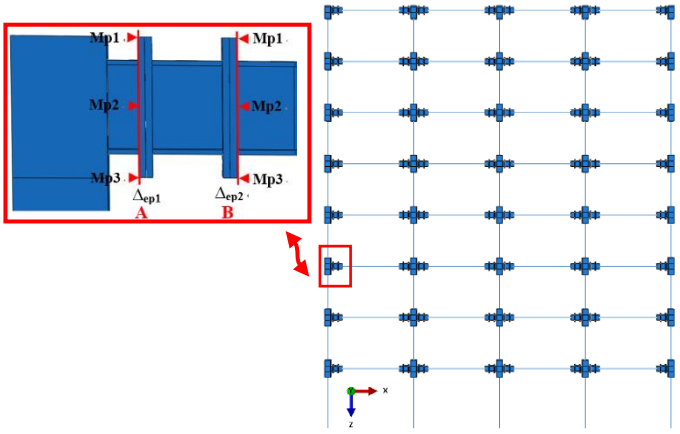

Fig. 35 Schematic diagram of measuring point selection for the end-plate residual displacement

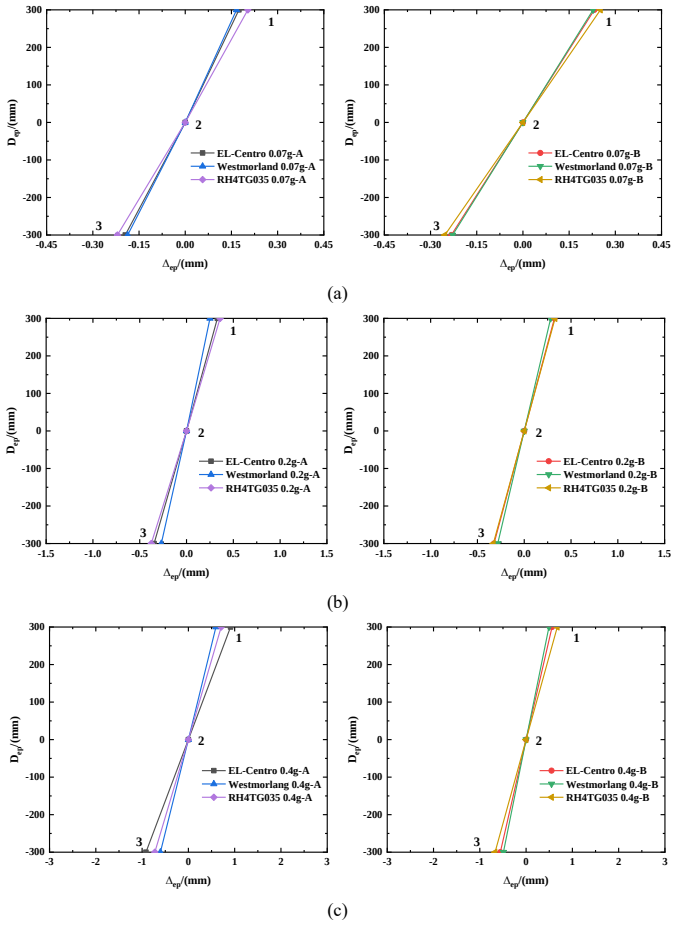

Fig. 36 Residual displacement curves of the replaceable beam segment under seismic action: (a) Frequent earthquake, (b) Moderate earthquake, (c) Rare earthquake

Fig. 36 and Table 12 revealed that during seismic activity, both the residual rotation angle and the relative residual rotation angle of the end plate remained significantly below the installation tolerance limit for steel structure members, set at 0.15% rad. Consequently, the replacement of the energy dissipation beam section was feasible. However, under rare earthquake conditions, the maximum residual rotation angle of the end plate at positions A and B exceeded the installation tolerance limit of the steel structure members (0.15% rad). In contrast, the relative residual rotation angle remained below this limit. This suggests the limited replaceability of the energy dissipation beam segment.

In conclusion, if only the residual inter-story displacement angle of the structure was considered as the criterion for the replaceability of the energy dissipation beam segment, the structure clearly met the replaceability requirement under rare earthquake conditions. Nevertheless, when the rotation angle of the end plate between the replaceable beam segment and the steel beam surpassed the component installation tolerance limit, the replacement of the energy dissipation beam segment became challenging or unattainable. Therefore, it is crucial to consider both the overall and local residual deformations when assessing the structural replaceability.

Table 12
Residual rotation angle of the replaceable beam segment under seismic action

Seismic level	Seismic wave	Residual rotation angle at position A (% rad)	Residual rotation angle at position A (% rad)	Relative residual rotation angle between positions A and B (% rad)
Frequent earthquake	EL-Centro	0.0615	0.0774	0.0159
	Westmorland	0.0589	0.0760	0.0171
	RH4TG035	0.0706	0.0842	0.0136
	Average	0.0637	0.0792	0.0155
Moderate earthquake	EL-Centro	0.1127	0.1076	0.0049
	Westmorland	0.0867	0.0942	0.0075
	RH4TG035	0.1225	0.1099	0.0126
	Average	0.1073	0.1039	0.0083
Rare earth-quake	EL-Centro	0.3046	0.1862	0.1184
	Westmorland	0.1999	0.1637	0.0362
	RH4TG035	0.2389	0.2242	0.0147
	Average	0.2478	0.1914	0.0564

6. Conclusions

In this study, a beam-column joint featuring a reduced-beam section and a replaceable energy dissipation beam segment was meticulously designed. After the design phase, a comprehensive quasi-static analysis was conducted on the joint and the single-story, single-span steel frame incorporating this novel joint. The analysis included exploring the seismic performance, failure modes, opening clearance, and end plate rotation angles. These findings laid the groundwork for streamlining an overall plane frame. Moreover, multi-scale models for both the RBSSF and RSF structures were crafted. Elastoplastic time-history analyses were then employed to scrutinize the replaceability of the beam segment and ascertain the practical requirements for replacement. The primary conclusions derived from this study are summarized as follows:

1. The hysteresis curve of the joint featuring a replaceable low-yield-point energy dissipation segment exhibited notable completeness, signifying high ductility and effective energy dissipation with a robust plastic deformation capacity.

2. Throughout the entire loading process, damage and plastic development predominantly occurred in the replaceable low-yield-point energy dissipation beam. The minimal opening clearance of the end plate ensured close bolt contact, fostering coordinated deformation between the end plates. Consequently, a stable force transfer mechanism was established in this connection mode. Additionally, the simplified joint model adeptly replicated the mechanical and deformation characteristics of the refined joint model.

3. In response to frequent, moderate, and rare earthquakes with a Richter magnitude of 8, the time-history curves depicting the development trends of the top floor displacement and base shear force in both the RBSSF and RSF structures exhibited similarities. The maximum inter-story displacement angles in both structures adhered to the code requirements. Notably, under frequent and moderate earthquakes, the RBSSF structure, characterized by reduced beam sections, demonstrated larger maximum top floor displacement and inter-story displacement angles than the RSF structure. This difference can be attributed to the RBSSF's overall lower stiffness. Conversely, the RBSSF structure exhibited smaller maximum top floor displacement and inter-story displacement angles during rare earthquakes than the RSF structure. Furthermore, the maximum base shear force in the RBSSF structure was consistently lower than that in the RSF structure under all earthquake scenarios, highlighting the superior seismic performance of the RBSSF structure.

4. The residual inter-story displacement angle of the RBSSF structure during frequent, moderate, and rare earthquakes with a Richter magnitude of 8 met the prescribed limits for the residual inter-story displacement angle in the performance target. Additionally, the residual rotation angle of the end plate in the replaceable energy dissipation beam segment satisfied the replaceable deformation limit under frequent and moderate earthquakes. However, under rare earthquakes, the residual angle of the end plate in the replaceable energy dissipation beam section slightly exceeded the limit, posing challenges for replacing the energy dissipation beam segment. Both overall residual and local

residual deformations should be considered when assessing replaceability.

5. This study investigated the seismic performance and replaceability of a reduced-beam-section beam-column joint with a replaceable energy dissipation beam segment through numerical simulations. Future research should further validate these results by using model tests.

Acknowledgments

This study was supported by the Shandong Natural Science Foundation Project (ZR2021ME239).

References

[1] David, B., "The dilemma of existing buildings: Private property, public risk", SPUR (San Francisco Bay Area Planning and Urban Research Association), 2009.
[2] Zhou, Y., Wu, H. and Gu, A.Q., "Earthquake engineering: from earthquake resistance, energy dissipation, and isolation, to resilience", Engineering Mechanics, 36(6), 1-12, 2019. (In Chinese)
[3] Lü, X.L., Quan, L.M. and Jiang, H.J., "Research trend of earthquake resilient structures seen from 16WCEE", Earthquake Engineering and Engineering Dynamics, 37(03), 1-9, 2017. (In Chinese)
[4] Zhou, Y. and Lü, X.L., "State-of-the-art on rocking and self-centering structures", Journal of Building Structures, 32(9), 1-10, 2011. (In Chinese)
[5] Lü, X.L. and Chen, C., "Research progress in structural systems with replaceable members", Earthquake Engineering and Engineering Dynamics, 34(01), 27-36, 2014. (In Chinese)
[6] Housner, G.W., "The behavior of inverted pendulum structures during earthquakes", Bulletin of the Seismological Society of America, 53(2), 403-417, 1963.
[7] Wada, A., Qu, Z., Ito, H., Motoyui, S., Sakata, H. and Kasai, K., "Seismic Retrofit Using Rocking Walls and Steel Dampers", ATC and SEI Conference on Improving the Seismic Performance of Existing Buildings and Other Structures, 2009.
[8] Zhang, F.W., Li, X.M., Xu, Q.F., Gong, C.C., Chen, X. and Liu, Q., "Experimental study on seismic behavior of frame-rocking wall structure", Journal of Building Structures, 36(8), 73-81, 2015. (In Chinese)
[9] Li, Y.W., Li, G.Q., Jiang, J. and Wang, Y.B., "Seismic performance improvement of tension-only-braced frames with energy-dissipative rocking columns", Engineering Structures, 196, 109286, 2019.
[10] Jia, M.M., Zhou, Z., Lü, D.G. and Yang, N., "Demand stiffness ratio and earthquake response analysis of rocking truss-steel frame system", Engineering Mechanics, 35(10), 66-74, 2018. (In Chinese)
[11] Zhang, W.J., Li, G.Q. and Ssun, F.F., "Seismic behavior of rocking-truss-frame with dampers", Journal of Tongji University (Natural Science), 47(9), 1235-1243, 2019. (In Chinese)
[12] Dong, J.Z., Zhang, F.W. and Li, X.M., "Experimental study on the seismic performance of frame-prestressed rocking wall structures", Engineering Mechanics, 36(4), 167-176, 2019. (In Chinese)
[13] Du, Y.F. and Wu, D.Y., "Performance analysis of light energy dissipative rocking frame designed on the basis of stiffness demand", China Civil Engineering Journal, 47(1), 24-35, 2014. (In Chinese)
[14] Chen, S.C., Liu, B.T., Cheng, S.N. and Yan, W.M., "Residual drift response analysis and calculated method of self-centering rocking wall structural systems", Journal of Guangzhou University (Natural Science Edition), 15(1), 45-50, 2016. (In Chinese)
[15] Lin, Y.C., Sause, R. and Ricles, J., "Seismic Performance of a Large-Scale Steel Self-Centering Moment-Resisting Frame: MCE Hybrid Simulations and Quasi-Static Pushover Tests", Journal of Structural Engineering, 139(7), 1227-1236, 2013.
[16] Lin, Y.C., Sause, R. and Ricles, J.M., "Seismic Performance of Steel Self-Centering, Moment-Resisting Frame: Hybrid Simulations under Design Basis Earthquake", Journal of Structural Engineering, 139(11), 1823-1832, 2013.
[17] Holden, T., Restrepo, J. and Mander, J.B., "Seismic Performance of Precast Reinforced and Prestressed Concrete Walls", Journal of Structural Engineering, 129(3), 286-296, 2003.
[18] Smith, B.J., Kurama, Y.C. and Mcginnis, M.J., "Behavior of Precast Concrete Shear Walls for Seismic Regions: Comparison of Hybrid and Emulative Specimens", Journal of Structural Engineering, 139(11), 1917-1927, 2013.
[19] Wu, H., Lü, X.L., Jiang, H.J., Shi, W.X. and Li, J.B., "Experimental study on seismic performance of prestressed precast concrete shear walls", Journal of Building Structures, 37(5), 208-217, 2016. (In Chinese)
[20] Gu, A.Q., Zhou, Y., Xiao, Y., Li, Q.W. and Qu, G., "Experimental study and parameter analysis on the seismic performance of self-centering hybrid reinforced concrete shear walls", Soil Dynamics & Earthquake Engineering, 116, 409-420, 2019.
[21] Xu, L.H., Zhang, G. and Yan, X.T., "Seismic performance study of reinforced concrete frame with self-centering braces", Engineering Mechanics, 37(2), 90-97, 2020. (In Chinese)
[22] He, H.X., Liao, L.C. and Shi, T., "Damping performance experiment and damage analysis of replacement connection with low-yield-point steel", Advanced Steel Construction, 17(2), 169-180, 2021.
[23] Chen, Y.Y. and He, X.Z., "Tests on moment resistant frame connection with replaceable angles", Steel Construction (Chinese & English), 35(8), 1-16, 2020.
[24] Wang, M., Zhang, C.Y., Sun, Y. and Dong, K.P., "Seismic performance of steel frame with replaceable low yield point steel connection components and the effect of structural fuses", Journal of Building Engineering, 47, 103862, 2022.
[25] Xu, L.H., Xie, X.S. and Li, Z.X., "Mechanics and performance study of self-centering variable damping energy dissipation brace", Engineering Mechanics, 35(1), 201-208, 2018. (In Chinese)
[26] Jiang, Z.Q., Yang, X.F., Zhang, A.L., Niu, Z.Y. and Wang, Q., "Experimental study on energy consuming devices for earthquake-resilient prefabricated cross joints", Journal of Building Structures, 41(1), 15-23, 2020. (In Chinese)
[27] Zhang, Y.X., Liu, A.R., Zhang, A.L. and Liu, X.C., "Seismic performance analysis of a resilient prestressed steel frame with intermediate column containing friction dampers", Advanced Steel Construction, 13(3), 241-257, 2017.
[28] Luo, J.L., "Study on seismic performance of buckling restrained steel beam-column connections based on damage control", Shandong University, 2018. (In Chinese)
[29] Shen, Y.L., Christopoulos, C., Mansour, N. and Tremblay, R., "Seismic design and performance of steel moment-resisting frames with nonlinear replaceable links," Journal of Structural Engineering, 137(10), 1107-1117, 2011.
[30] Wang, J., "Experimental study on seismic behavior of replaceable steel beams in assembled RCS hybrid structures", Huaqiao University, 2017. (In Chinese)
[31] Zhang, A.L., Zhang, Y.X., Zhao, W. and Fei, C.C., "Pseudo dynamic tests for a resilient prefabricated prestressed steel frame", Journal of Vibration and Shock, 35(5), 207-215, 2016. (In Chinese)
[32] Castiglioni, C.A., Kanyilmaz, A. and Calado, L., "Experimental analysis of seismic resistant composite steel frames with dissipative devices", Journal of Constructional Steel Research, 76, 1-12, 2012.
[33] Oh, S.H., Kim, Y.J. and Ryu, H.S., "Seismic performance of steel structures with slit dampers", Engineering Structures, 31(9), 1997-2008, 2009.
[34] Shao, T.F. and Chen, Y.Y., "Experimental study on steel H-beams with replaceable energy dissipation angle", Journal of Building Structures, 37(7), 38-45, 2016. (In Chinese)
[35] Hu, Y.Y., "Research on seismic damage-control fuses used in high-strength steel beam-to-column joint", Institute of Engineering Mechanics, China Earthquake Administration, 2017. (In Chinese)
[36] He, H.X., Chen, K. and Li, R.F., "Seismic analysis of replaceable steel connection with low yield point metal", Journal of Vibration, Measurement and Diagnosis, 36(6), 1050-1056, 2016. (In Chinese)
[37] Wang, M., Bi, P., Yang, W.G. and Wu, Z.Z., "Study on mechanical behavior of ductile steel frame connection with low yield point steel 'structural fuse'", Journal of Building Structures, 40(11), 90-101, 2019. (In Chinese)
[38] Chi, H. and Liu, J., "Seismic behavior of post-tensioned column base for steel self-centering moment resisting frame", Journal of Constructional Steel Research, 78, 117-130, 2012.
[39] GB50017-2014. "Standard for design of steel structures", China Planning Publishing House, 2014. (In Chinese)
[40] GB50011-2010. "Code for seismic design of buildings", China Building Industry Press, 2010. (In Chinese)
[41] AISC358-16. "Prequalified Connections for Special and Intermediate Steel Moment Frames for Seismic Applications", American Institute of Steel Construction, 2016.
[42] Liu, W.T., "The GTN damage model with combined hardening rule", Beijing Jiaotong University, 2014. (In Chinese)
[43] ANSI/AISC 341-05. "Seismic Provisions for Structural Steel Buildings", American Institute of Steel Construction, 2005.
[44] Zhang, A.L., Guo, Z.P., Liu, X.C. and Jiang, Z.Q., "Experimental study on aseismic behavior of prefabricated steel-frame-joints with Z-shaped cantilever-beam splicing", Engineering Mechanics, 34(8), 31-41, 2017. (In Chinese)
[45] JGJ/T101-2015. "Specification for seismic test of buildings", China Building Industry Press, 2015. (In Chinese)
[46] Shi, Y.J., Wang, M., Wang, Y.Q., "Analysis on seismic behavior of overall steel frame with different welded connection constructions", Engineering Mechanics, 29(11), 71-79, 2012. (In Chinese)
[47] Wang, M., "Damage and degradation behaviors of steel frames under severe earthquake", Tsinghua University, 2013. (In Chinese)
[48] Hong, W., "Analysis of lateral collapse-resistance of steel frame based on beam-to-column connections and buckling restrained brace", Southeast University, 2019. (In Chinese)
[49] ATC-63. "Quantification of Building Seismic Performance Factors", ATC-63 Project Report, 2008.
[50] SEAOC. "Vision 2000: Performance based seismic engineering of building", Structural Engineers Association of California, 1995.
[51] FEMA P 58-1, "Seismic Performance Assessment of Buildings", Applied Technology Council and Federal Emergency Management Agency, 2012.
[52] Uma, S.R., Pampanin, S. and Christopoulos, C., "Development of Probabilistic Framework for Performance-Based Seismic Assessment of Structures Considering Residual Deformations", Journal of Earthquake Engineering, 14(7), 1092-1111, 2010.
[53] Wu, D.Y. and Lü, X.L., "Probabilistic performance assessment of self-centering dual systems", Journal of Building Structures, 38(8), 14-24, 2017. (In Chinese)
[54] Chen, Y.Y., He, X.Z., Ke, K. and Chen, Y.S., "Characteristics and technical issues on structural systems with replaceable damage-concentrated elements", Journal of Building Structures, 37(2), 1-10, 2016. (In Chinese)